

## Compact tool for deposition of composition spread alloy films

Deepika Priyadarshini, Petro Kondratyuk, James B. Miller, and Andrew J. Gellman

Citation: *Journal of Vacuum Science & Technology A* **30**, 011503 (2012); doi: 10.1116/1.3664078

View online: <http://dx.doi.org/10.1116/1.3664078>

View Table of Contents: <http://scitation.aip.org/content/avs/journal/jvsta/30/1?ver=pdfcov>

Published by the AVS: Science & Technology of Materials, Interfaces, and Processing

---

### Articles you may be interested in

[Growth behavior and intrinsic properties of vapor-deposited iron palladium thin films](#)

*J. Appl. Phys.* **103**, 046108 (2008); 10.1063/1.2875306

[On the use of alloying elements for Cu interconnect applications](#)

*J. Vac. Sci. Technol. B* **24**, 2485 (2006); 10.1116/1.2357744

[Composition and structure of Cu-based nanoicosahedral phase in Cu-Zr-Ti-Pd alloy](#)

*Appl. Phys. Lett.* **87**, 211918 (2005); 10.1063/1.2135143

[Collision as a way of forming bimetallic nanoclusters of various structures and chemical compositions](#)

*J. Chem. Phys.* **123**, 184505 (2005); 10.1063/1.2104487

[Annealing enhanced hydrogen absorption in nanocrystalline Pd/Au sensing films](#)

*J. Appl. Phys.* **97**, 124301 (2005); 10.1063/1.1927690

---



## Instruments for Advanced Science

 <p><b>Gas Analysis</b></p> <ul style="list-style-type: none"><li>dynamic measurement of reaction gas streams</li><li>catalysis and thermal analysis</li><li>molecular beam studies</li><li>dissolved species probes</li><li>fermentation, environmental and ecological studies</li></ul>	 <p><b>Surface Science</b></p> <ul style="list-style-type: none"><li>UHV TPD</li><li>SIMS</li><li>end point detection in ion beam etch</li><li>elemental imaging - surface mapping</li></ul>	 <p><b>Plasma Diagnostics</b></p> <ul style="list-style-type: none"><li>plasma source characterization</li><li>etch and deposition process reaction</li><li>kinetic studies</li><li>analysis of neutral and radical species</li></ul>	 <p><b>Vacuum Analysis</b></p> <ul style="list-style-type: none"><li>partial pressure measurement and control of process gases</li><li>reactive sputter process control</li><li>vacuum diagnostics</li><li>vacuum coating process monitoring</li></ul>
--	---	---	---

Contact Hiden Analytical for further details:  
**W** [www.HidenAnalytical.com](http://www.HidenAnalytical.com)  
**E** [info@hiden.co.uk](mailto:info@hiden.co.uk)  
**CLICK TO VIEW** our product catalogue

# Compact tool for deposition of composition spread alloy films

Deepika Priyadarshini, Petro Kondratyuk, James B. Miller, and Andrew J. Gellman<sup>a)</sup>  
National Energy Technology Laboratory, US Department of Energy, P.O. Box 10940, Pittsburgh,  
Pennsylvania 15236 and Department of Chemical Engineering, Carnegie Mellon University,  
Pittsburgh, Pennsylvania 15213

(Received 11 August 2011; accepted 27 October 2011; published 29 November 2011)

Composition spread alloy films (CSAFs) are combinatorial materials libraries that contain broad, continuous composition ranges of binary or higher-order alloys on a single, compact substrate. When characterized for composition and functional properties using spatially resolved methods, CSAF libraries enable rapid determination of composition-property relationships across broad continuous regions of alloy composition space. In this report, we describe the design and operation of a novel offset filament deposition tool for preparation of CSAFs. The spatial distribution of individual alloy component fluxes to the substrate surface, and thus the film composition across the substrate, is controlled by the location and temperature of chemically distinct evaporative line sources. The tool can be used for quantitative deposition of thin ( $\leq 100$  nm) CSAFs with up to four components. The authors demonstrate the performance of the tool by applying it to preparation of 100 nm thick Pd-Cu CSAFs, with lateral composition gradients that span the range  $\text{Cu}_{0.05}\text{Pd}_{0.95}$  to  $\text{Cu}_{0.95}\text{Pd}_{0.05}$ , on a 12 mm diameter Mo(110) substrate. © 2012 American Vacuum Society. [DOI: 10.1116/1.3664078]

## I. INTRODUCTION

The conventional approach to establishing composition-property relationships in multicomponent materials is to prepare and carefully characterize a series of single-composition samples. However, sampling complex, multidimensional composition spaces with high resolution can be both time- and cost-prohibitive. High throughput approaches, based on preparation and parallel characterization of combinatorial materials libraries, have been developed to accelerate the process of materials discovery and optimization.<sup>1,2</sup> Such methods are equally well applied to fundamental scientific problems in surface science and materials science that require the measurement of properties across broad, continuous regions of composition space. As an example, surface segregation in  $\text{A}_x\text{B}_{1-x}$  alloys, which is of considerable technical interest for applications as diverse as catalysis and corrosion control, is usually characterized at only at a limited number of discrete compositions, in spite of the fact that a comprehensive understanding of segregation requires study across the entire composition space,  $x=0 \rightarrow 1$ .<sup>3</sup> Development of tools and methodologies for efficient preparation and property characterization of materials libraries provides a foundation for high throughput study of segregation and other phenomena in multicomponent materials.

The combinatorial approach has been successfully applied in several scientific domains. Combinatorial chemistry has long been used for discovery and optimization in pharmaceutical research.<sup>4,5</sup> Combinatorial approaches have also resulted in discovery of new materials for applications as catalysts, polymers, superconductors, magnetic materials, structural materials, and coatings.<sup>6-10</sup> These methods have been applied to the study of a wide variety of materials properties including stress, hardness, and catalytic activity.<sup>11-13</sup>

Design of the combinatorial sample library is a key to successful high throughput experimentation. The composition spread alloy film (CSAF) sample platform has been applied to high throughput study of inorganic materials.<sup>6,9,10,14-17</sup> The CSAF, shown schematically in Fig. 1, is a sample library with a composition that is continuously variable across a single, compact substrate. For a ternary alloy, all possible compositions can be present on the surface of a single CSAF. For higher order alloys, the CSAF sample is a 2D surface cut through multidimensional composition space. Alternatively, preparation parameters can be controlled to zoom in on any 2D subspace of composition space. Spatially resolved measurements of composition and of functional properties across the CSAF surface enable rapid construction of composition-property relationships for both materials understanding and optimization.

Composition spread alloy films are typically prepared using a set of chemically distinct, single-component physical vapor deposition sources. There are several strategies for controlling the flux distribution at the substrate surface, and ultimately the lateral distribution in the CSAF composition, as shown in Fig. 2. One approach to deposition of CSAFs, shown in Fig. 2(a), uses sources that give a uniform flux of individual components to the substrate and a contact mask that slides across the substrate surface to vary the effective deposition time, and thus thickness, at different locations on the substrate.<sup>18-20</sup> Components are deposited individually in the form of wedges and intermixing is accomplished by subsequent annealing of the multilayer structure. A second and related approach, as shown in Fig. 2(b), uses multiple sources operating simultaneously with shadow masks between the sources and the substrate.<sup>17,21-23</sup> The masks shadow the substrate from portions of the source; thus varying the deposition flux across the substrate. The shadow mask approach has the advantage of allowing *simultaneous* deposition of multiple components, obviating the need for subsequent intermixing. A third method, as shown in Fig. 2(c), is to use sources positioned at

<sup>a)</sup>Author to whom correspondence should be addressed; electronic mail: gellman@cmu.edu

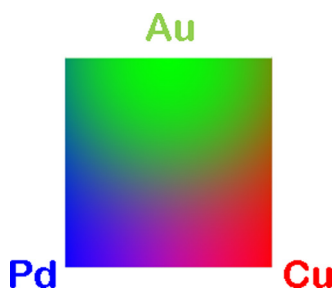


FIG. 1. (Color online) Three component CSAF containing a broad, continuous distribution of the possible compositions of a ternary  $\text{Cu}_x\text{Au}_y\text{Pd}_{1-x-y}$  alloy on a single substrate.

points that are offset relative to the substrate to give inherent gradients in their fluxes to the substrate surface.<sup>16,24</sup>

In this paper, we describe the design, operation and performance of a simple compact offset filament deposition tool for preparing CSAFs with up to four components. The tool has been developed over the past few years in our laboratory; in its current design, the tool is capable of repeatable, quantitative production of thin ( $\leq 100$  nm) CSAFs on substrates that are up to  $\sim 12$  mm in diameter. The tool can be used to deposit metals that are evaporable at temperatures up to  $\sim 1500$  K and can produce fluxes that vary by an order of magnitude across the substrate surface. When component fluxes are equal at the center of the substrate, the composition of a binary CSAF can range from  $\sim A_{0.05}B_{0.95}$  to  $A_{0.95}B_{0.05}$  across the 12 mm substrate.

## II. OFFSET FILAMENT CSAF DEPOSITION TOOL

### A. Deposition geometry

Figure 3(a) is a schematic diagram that shows the deposition geometry of the CSAF deposition tool. Four chemically

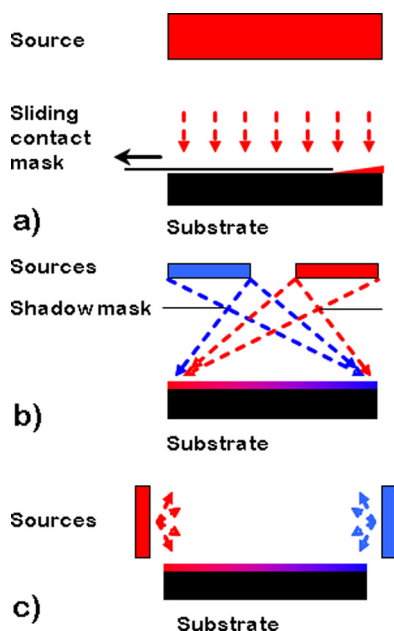


FIG. 2. (Color online) Three methods for deposition of CSAFs. (a) Deposition of individual components in wedges using a sliding contact mask. (b) Simultaneous deposition of multiple components using shadow masks to form the composition gradients. (c) Offset positioning of sources to generate inherent flux distributions across the substrate surface.

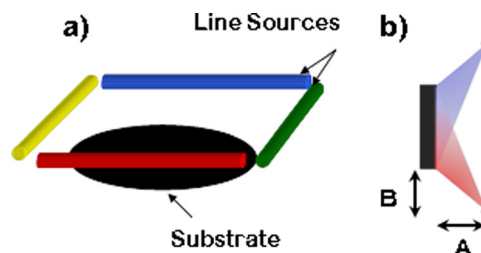


FIG. 3. (Color online) (a) Schematic of the offset filament CSAF deposition geometry with four different line sources offset from the edge of the substrate. (b) Side view of the deposition geometry with two line sources depositing a binary CSAF. Line sources are placed 5 mm ( $A$ ) from the substrate in the normal direction and 4 mm ( $B$ ) from the edge of a 12 mm substrate.

distinct line sources are located at positions near the substrate, but offset from its centerline. Conceptually, this is equivalent to the deposition method illustrated in Fig. 2(c). With this arrangement, the flux to the substrate varies with distance across the substrate—deposition rates for a given component are highest at points closest to its source. The line sources, each 14 mm long, are positioned  $\sim 4$  mm from the edge and  $\sim 5$  mm above the 12 mm diameter substrate. As we will show later, the longer the line source relative to substrate dimensions, the more uniform the flux to the substrate in the direction parallel to the source. Distances from the line source to the edge of the substrate can be tailored to deliver a desired CSAF composition distribution. Each line source can contain a different evaporant and can be heated independently to different temperatures to control fluxes. The entire assembly is very compact and can be mounted onto a 2.75" CF flange.

### B. Line sources

Quantitative deposition of the CSAF requires precise control of the geometry of the sources and the substrate, and uniformity of evaporant flux from each point along each line source. Maintaining constant temperature along the length of the line source is the key to uniformity and repeatability of evaporant flux. To achieve uniform temperature, we use thermal evaporative sources of our own design. The critical component if the line sources is the evaporant heating bar, shown in Fig. 4. The heating bar is a 14 mm-long Mo tube (3.2 mm O.D.  $\times$  0.9 mm I.D.) with a 0.5 mm slot along its outer edge into which the evaporant material is press fit. We typically use 0.5 mm diameter evaporant wires, but other dimensions or form factors should work equally well. The primary role of the Mo bar is to provide a thermally conductive mass that distributes heat along its length and keeps the entire source at a uniform temperature. The tube has been made from Mo or Ta to minimize the opportunity for alloying of the evaporant materials with the tube.<sup>25,26</sup>

The line sources are heated using a 0.38 mm diameter W or Ta wire located inside the Mo heating block and electrically insulated from the block by a ceramic tube (0.9 mm O.D.  $\times$   $\sim 0.38$  mm I.D.). The diameters of the heater wire and ceramic tube are not critical to line source performance

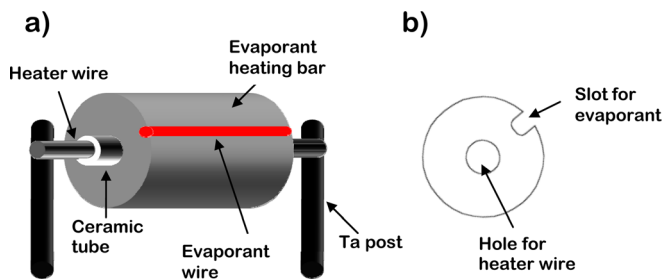


FIG. 4. (Color online) (a) Thermal evaporative line source. A ceramic tube and heater wire are both located on the axis of the evaporant heating bar. At either end, the heater wire is spot welded to Ta posts for support. (b) Side view of the evaporant bar with the hole for ceramic tube and heater wire and a slot for the metal evaporant wire. The evaporant wire is press fit into the slot.

and other dimensions should work equally well. In operation, the W or Ta wire is heated resistively. The ceramic tube prevents current from passing through the source block, and thus minimizes the power needed to achieve the desired source temperature.

### C. Line source mounting block

The second requirement for repeatable, quantitative deposition is precise location of the line sources with respect to one another and with respect to the substrate. The four line sources are mounted onto a water-cooled Cu mounting block [Fig. 5(a)]. They are oriented in a square configuration, as shown in Fig. 3, such that they are  $\sim 4$  mm from the edge of the 12 mm substrate and  $\sim 5$  mm in front of the substrate surface. Heater wires are spot welded to pairs of thick (0.76 mm diameter) Ta posts. The Ta posts pass through ceramic tubes embedded into the Cu block. Four thermocouple pairs, insulated by ceramic tubes, also pass through the mounting block. The thermocouples are spot welded to line sources' evaporant bars; they are used for temperature control of the individual line sources during deposition of the CSAF. We have used type K, R and C thermocouples to evaporate Cu, Pd and Au. Types R or C are preferred because we observed partial evaporation of type K thermocouples at temperatures of  $\sim 1500$  K. The Cu mounting block has a water inlet/outlet on the bottom side to allow cooling during operation.

The original design of the mounting block included shields that shadowed the four line sources from one another to prevent cross-contamination. We have found; however, that these shields are not necessary for the deposition of Cu, Pd and Au. The deposition tool is built on a 2.75" CF cluster flange with five 1.33" CF mini-flange ports. The central (on-axis) mini-flange is used for the tube that supports the source and provides cooling water to the Cu mounting block. The four other mini flanges are used for thermocouple and power feedthroughs. The 2.75" cluster flange can be mounted directly to a 2.75" CF flange on a standard UHV chamber [Fig. 5(b)] or to a small manipulator to allow precise positioning of the tool within the chamber.

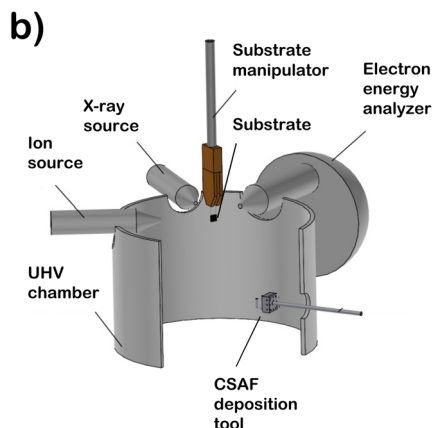
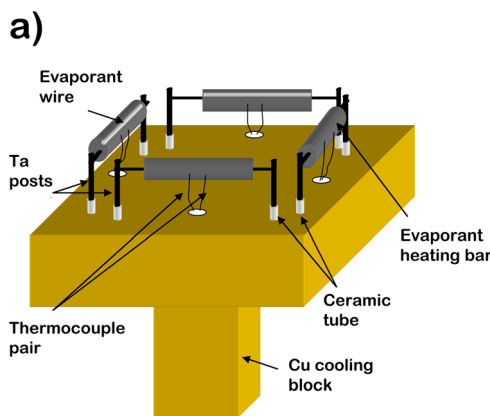


FIG. 5. (Color online) (a) Schematic of the offset filament CSAF deposition tool. Four line sources are mounted in a square configuration on a Cu block. Ta posts passing through ceramic tubes support each of the four line sources. A thermocouple pair is spot welded to each of the line sources. (b) Schematic of the UHV chamber in which the CSAF source is mounted. Deposition is performed by positioning the substrate in the lower level and in front of the source. Substrate cleaning and CSAF analysis is performed in the upper level of the chamber.

### D. Line source temperature control

Line source heater wires are connected to programmable power supplies (Lambda GENH 8-90-U) and their temperatures are controlled by LABVIEW software. Using the materials and the mounting geometry described above, we find that heating to temperatures in the range 1300 – 1500 K requires input power of 10 – 20 W per line source.

Operation of the CSAF deposition tool requires heating of the individual line sources to temperatures that deliver the desired deposition rates across the substrate surface. For example, deposition of an alloy with equal compositions of all components ( $A_{0.25}B_{0.25}C_{0.25}D_{0.25}$ ) at the center of the substrate requires the identification of four different line source temperatures that yield equal fluxes at the center of the substrate. To access a specific subspace of composition space, the line sources can be operated at temperatures that deliver different fluxes.

Before use for deposition, the CSAF deposition tool requires extensive degassing in vacuum to eliminate the deposition of contaminants onto the substrate. This requires heating of the line sources for long time periods ( $\sim 5$  hs) at

temperatures comparable to or greater than those being used for CSAF deposition. It is important to note that the compact geometry of the source and the proximity of the offset filaments to the substrate induce non-negligible heating of the substrate by 100 – 150 K during deposition. Of course, the temperature rise will also depend on the method used to mount the substrate and its cooling efficiency.

### III. MODELING OF LINE SOURCE CHARACTERISTICS

The preparation of a CSAF requires deposition of the individual components with flux gradients across the substrate surface. In our offset filament design, source-substrate geometry creates the flux gradient—points closer to the line source receive higher evaporant flux than those far from the source. A single source creates a film of variable thickness across the substrate. Two or more such line sources create an alloy film with variable composition across the substrate. Films can also be made with both composition and thickness gradients across the substrate.

The flux at a given point on the substrate from a given point on the line source depends upon the distance between them as shown in Fig. 6. Only the perpendicular component of flux at the substrate surface contributes to the film deposition rate. The total flux at any point  $(x_0, y_0)$  on the substrate is obtained by integrating over the entire length  $(L)$  of the line source.

$$F(x_0, y_0) \propto \int_{-L/2}^{L/2} \frac{\bar{R}(y; x_0, y_0, A, B) \cdot \hat{z}}{|\bar{R}(y; x_0, y_0, A, B)|^3} dy. \tag{1}$$

In this equation,  $\bar{R}(y; x_0, y_0, A, B)$  is the vector between a point  $(x_0, y_0)$  on the substrate and a point at position  $y$  along the line source which is located at a distance  $B$  from the edge of the substrate and positioned at a height  $A$  above the substrate plane. The term  $\hat{z}$  is the unit vector normal to the substrate surface, and the dot product,  $\bar{R} \cdot \hat{z}$ , incorporates the angle dependence of the flux into equation 1. For an infinite length

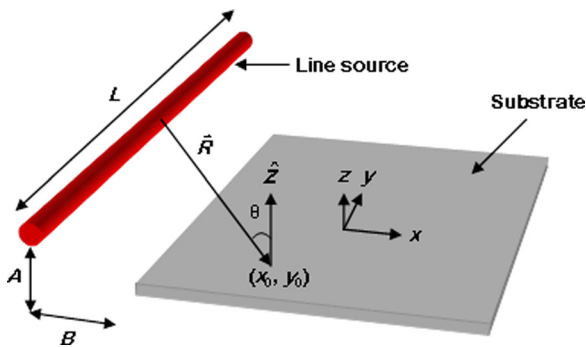


FIG. 6. (Color online) Deposition geometry for a single line source;  $x$  is the gradient direction,  $y$  is the direction parallel to the line source and  $z$  is the direction normal to the substrate. The line source is placed at a distance  $A$  from the substrate in the  $z$  direction and a distance  $B$  from the edge of the substrate in the  $x$  direction.  $R$  is the distance between any point on the line source and any point  $(x_0, y_0)$  on the substrate.  $\theta$  is the angle between  $\bar{R}$  and  $\hat{z}$ .

line source, the flux at the substrate is  $\propto R_{min}^{-2}$  where  $R_{min}$  is the minimum distance between the point  $(x_0, y_0)$  on the substrate and the line source,  $R_{min} = |\bar{R}(y_0; x_0, y_0, A, B)|$ .

A line source in this configuration creates a flux gradient across the substrate in the  $x$  direction with minor variation in the  $y$  direction. Figure 7(a) displays the calculated relative flux gradient across a 12 mm x 12 mm square substrate from a 14 mm long line source located at  $A = 5$  mm above the substrate and  $B = 4$  mm from the edge of the substrate as shown in Fig. 6. The flux variation in the  $y$  direction depends on the length of the line source  $(L)$  relative to substrate dimensions; for the hypothetical case of an infinite line source, the flux does not depend on  $y$ . As expected, because the source has finite length, the flux at any constant value of  $x$  [Fig. 7(a)] varies in the  $y$  direction with a maximum at the center of the substrate ( $y = 0$ ). Figure 7(b) shows the composition profile that results when two opposing line sources are operated such that the deposition rate from each is equal at the center of the substrate. The composition at constant  $x$  [Fig. 7(b)] is fairly insensitive to  $y$ , however, the total film thickness varies by  $\sim 20\%$  from the center of the substrate towards the edges in the  $y$  direction.

The spatial distribution of flux across the substrate and, therefore, the details of CSAF composition, can be varied by changing the source-substrate geometry. Figures 8(a) and 8(b) show the relative fluxes across substrate through its center point in the  $x$  and  $y$  directions, respectively, for different deposition geometries. The solid lines represent the “base case”

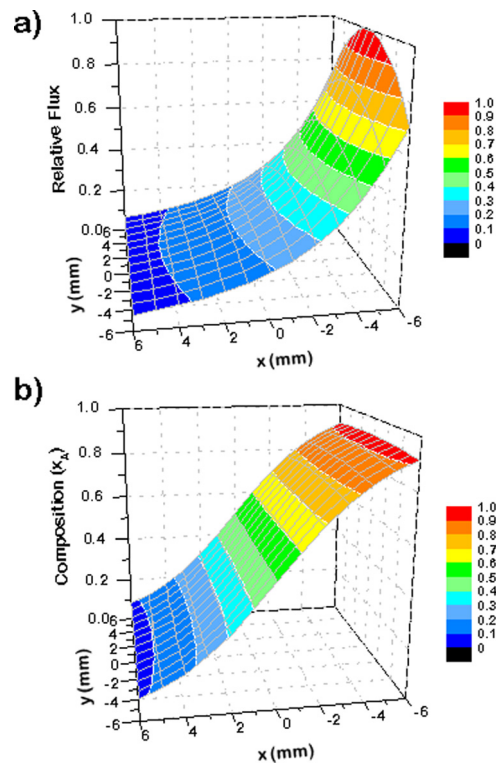


FIG. 7. (Color online) (a) Relative flux across the  $12 \times 12$  mm<sup>2</sup> substrate surface from a 14 mm line source. The flux varies monotonically in the  $x$  direction and symmetrically in the  $y$  direction with a maximum in the center at  $y = 0$ . (b) Composition profile for one component of a binary CSAF generated by simultaneous deposition from two opposing line sources.

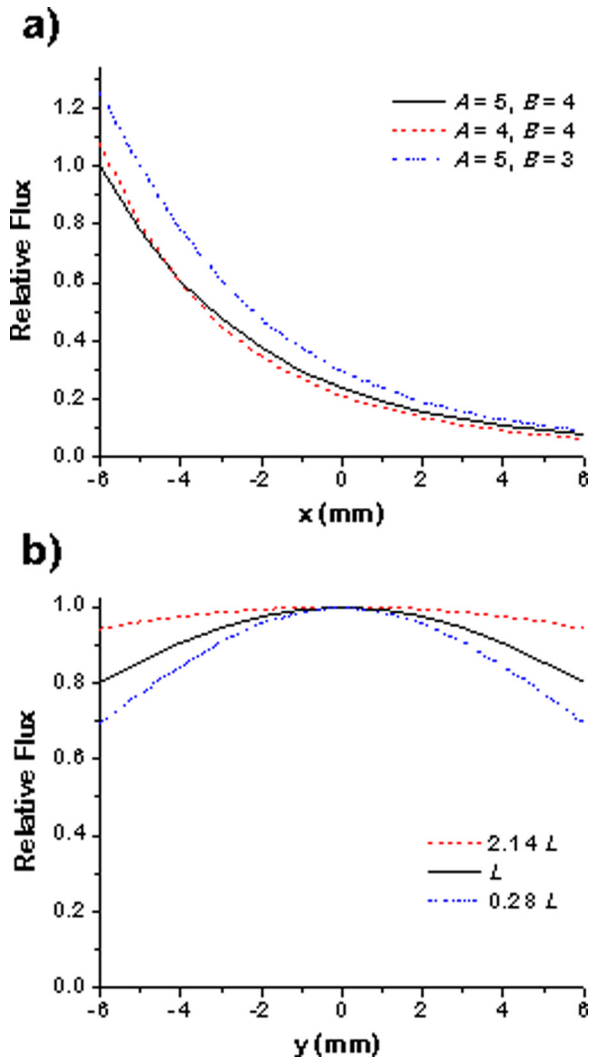


FIG 8. (Color online) Relative flux in  $x$  direction across the center of the substrate ( $y=0$ ) from a line source placed  $A$  distance above the substrate and  $B$  distance from the edge of the substrate. Flux varies across the substrate as the distance with respect to line source changes. (b) Relative flux in  $y$  direction across the center of the substrate ( $x=0$ ) from line sources of different length.

geometry described above ( $12 \times 12$  mm substrate,  $A=5$  mm,  $B=4$  mm,  $L=14$  mm). The dotted lines in Fig. 8(a) show flux across the substrate in the  $x$  direction as the offset between the line source and substrate is varied. The dotted lines in Fig. 8(b) shows the variation in flux as the length of the line source changes. As expected, flux is less sensitive to the  $y$ -location as the source becomes long relative to the width of the substrate.

#### IV. CSAF SOURCE OPERATION

##### A. Calibration of deposition rates

The offset filament deposition tool is housed in an ultra-high vacuum chamber that we have described previously.<sup>3,27</sup> The chamber is equipped with a monochromatic x-ray source (VG Scientific), a  $\text{He}^+$  ion gun (Specs IQE 12/38), and an energy analyzer (Specs PHOIBOS 150MCD) for characterization of near surface composition by  $x$  ray photo-

emission spectroscopy (XPS) and top surface composition by low energy ion scattering spectroscopy (LEIS).

In the examples presented here, we have deposited single component Pd and Cu wedges and  $\text{Cu}_x\text{Pd}_{1-x}$  CSAFs onto the surface of a 12 mm diameter Mo(110) single crystal using 14 mm long Pd and Cu line sources located  $\sim 5$  mm above the substrate ( $A$ ) and  $\sim 4$  mm offset from the edge of the substrate ( $B$ ) [Fig. 3(b)]. Before deposition, the substrate was cleaned by annealing at 1300 K in atmosphere of oxygen ( $\sim 10^{-8}$  Torr) followed by cycles of  $\text{Ar}^+$  ion bombardment at 300 K and annealing to 1300 K until C and O surface contaminants were less than  $\sim 15$  at. %. The Pd and Cu line sources were degassed by heating at 1200 K for  $\sim 5$  hs to remove any contaminants present on the Mo evaporant holder.

For quantitative deposition, the line sources must be calibrated individually by measuring their deposition rates as functions of location on the substrate surface. We performed the calibration by sequential deposition of a single component gradient at constant line source temperature. After each deposition cycle, XPS was used to characterize surface composition at a number of specific locations. The film thickness increased with each deposition cycle and the process was repeated several times until the substrate signal was almost undetectable using XPS.

Figure 9 shows the Pd and Mo XPS signals at the center of the Mo substrate as a function of Pd deposition time at a source temperature of 1400 K. The increase of the Pd signal and decrease of the Mo signal during deposition can be fit to an exponential Pd growth and Mo decay model<sup>28</sup>:

$$I_{\text{Pd}} = I_{\text{Pd}}^{\infty} \left[ 1 - \exp\left(\frac{-r_{\text{Pd}} \cdot t}{\lambda_{\text{Pd}} \cos \theta}\right) \right] \quad (2)$$

and

$$I_{\text{Mo}} = I_{\text{Mo}}^{\infty} \exp\left(\frac{-r_{\text{Pd}} \cdot t}{\lambda_{\text{Mo}} \cos \theta}\right), \quad (3)$$

where  $I_{\text{Pd}}$  and  $I_{\text{Mo}}$  are the Pd  $3d_{5/2}$  and Mo  $3d_{5/2}$  XPS intensities,  $I_{\text{Pd}}^{\infty}$  is the intensity observed from pure (infinitely thick) Pd,  $I_{\text{Mo}}^{\infty}$  is the intensity from the clean Mo substrate,  $t$  is the deposition time,  $\lambda_{\text{Pd}}=2.01$  nm is the mean free path of Pd  $3d_{5/2}$  photoelectrons in Pd,  $\lambda_{\text{Mo}}=2.15$  nm is the mean free path of Mo  $3d_{5/2}$  photoelectrons in Pd,  $\theta$  is the angle at which the analyzer collects the photoelectrons, and  $r_{\text{Pd}}$  is the Pd deposition rate.<sup>28</sup> The curves in Fig. 9 show the best fits of these equations to the Pd and Mo XPS intensities, yielding Pd deposition rates of  $0.070 \pm 0.005$  nm/min and  $0.078 \pm 0.005$  nm/min from the Pd and Mo XPS signals, respectively. Similar analyses (not shown) were performed at other locations on the substrate surface and for Cu deposition.

For simultaneous deposition of multiple components, it is important to determine the deposition rate from each source as a function of its operation temperature to choose source temperatures that deliver the desired relative deposition rates. This approach can be used to control the specific composition range of the CSAF. For example, a co-deposited binary alloy with equimolar composition, i.e.,  $\text{A}_{50}\text{B}_{50}$ , at the center of the

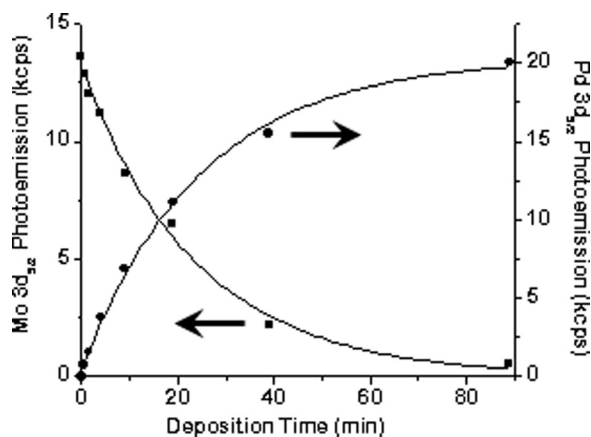


FIG. 9. Pd  $3d_{5/2}$  and Mo  $3d_{5/2}$  XPS signals at the center of the Mo(110) substrate as a function of deposition time. The solid lines represent the exponential fits to the Pd growth and Mo decay curves and are used to estimate the deposition rates.

substrate can be obtained, if the two line sources are operated at temperatures that deliver the same deposition rate at that point. Figure 10 shows the deposition rates for Cu and Pd at the center of the Mo(110) substrate as functions of temperature. The solid line represents the best fit of the Hertz-Knudsen equation to the measured deposition rates.<sup>29–31</sup> The Hertz-Knudsen equation relates evaporation rate to vapor pressure, temperature and atomic mass of the metal. The deposition rate is a fraction of the evaporation rate and is determined by the deposition geometry.

## B. Deposition of a $\text{Cu}_x\text{Pd}_{1-x}$ CSAF

Finally, we demonstrate the performance of the offset filament tool for preparation of a binary  $\text{Cu}_x\text{Pd}_{1-x}$  CSAF. The tool was configured with Pd and Cu line sources placed on opposite sides of a 12 mm diameter Mo(110) substrate, as shown in Fig. 3(b). A 100 nm thick  $\text{Cu}_x\text{Pd}_{1-x}$  CSAF was co-

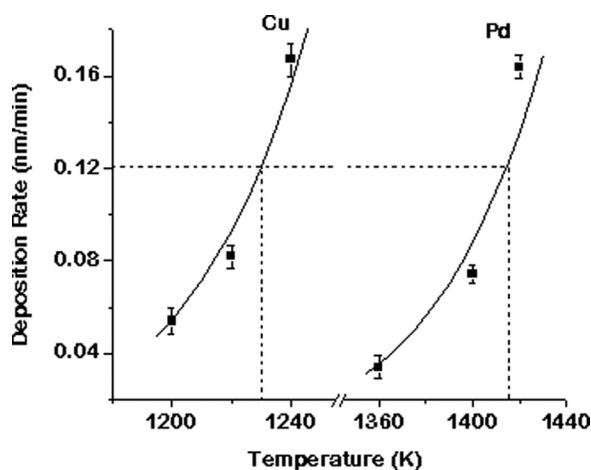


FIG. 10. Cu and Pd deposition rates as functions of line source temperature at the center of the Mo(110) substrate. The different source temperatures can be chosen to determine the relative fluxes of the different components and thus, generate the desired composition spread. The vertical dotted lines indicate the source temperatures chosen to give equal deposition rates of Cu and Pd at the center of the substrate.

deposited by operating the Cu line source at 1230 K and the Pd line source at 1415 K, represented by the dotted line in Fig. 10. These temperatures were chosen to give similar deposition rates for both metals at the center of the substrate. The bulk composition of the  $\text{Cu}_x\text{Pd}_{1-x}$  CSAF at specific locations on the substrate, expressed as fractional molar Cu content, was calculated from the Cu and Pd deposition rates:

$$x = \frac{r_{\text{Cu}}\rho_{\text{Cu}}}{r_{\text{Cu}}\rho_{\text{Cu}} + r_{\text{Pd}}\rho_{\text{Pd}}}. \quad (4)$$

In this equation,  $r_{\text{Cu}}$  and  $r_{\text{Pd}}$  are the deposition rates of Cu and Pd at the location of interest on the substrate surface,  $\rho_{\text{Cu}}$  and  $\rho_{\text{Pd}}$  are the molar densities of Cu and Pd, and  $x$  is the bulk mole fraction of Cu in the CSAF.

By comparing the bulk composition calculated from Eq. (4) with the results obtained from the model for the source operation described in Sec. III, we can validate the performance of the deposition tool. Figure 11 displays the Cu composition profile of the  $\text{Cu}_x\text{Pd}_{1-x}$  CSAF. The symbols (■) represent the Cu compositions in the bulk obtained from equation 4 using experimentally measured deposition rates. The lines represent the composition profiles estimated from the model for two different cases of substrate-source geometry. The solid line is the composition profile expected for a substrate positioned at the nominal design geometry ( $A = 5$  mm,  $B = 4$  mm). At the nominal geometry, the model matches the measurements reasonably well, with small under-prediction of  $x$  at high  $x$  and over-prediction at low  $x$ . The dashed line is the best fit of the model to the data using  $A$  and  $B$  as adjustable parameters. With  $A = B = 3.5$  mm, agreement between the model and experiment is excellent; the small difference between the two cases likely reflects uncertainty in our alignment of the substrate and the tool; we continue to refine our procedures to improve the accuracy of substrate placement.

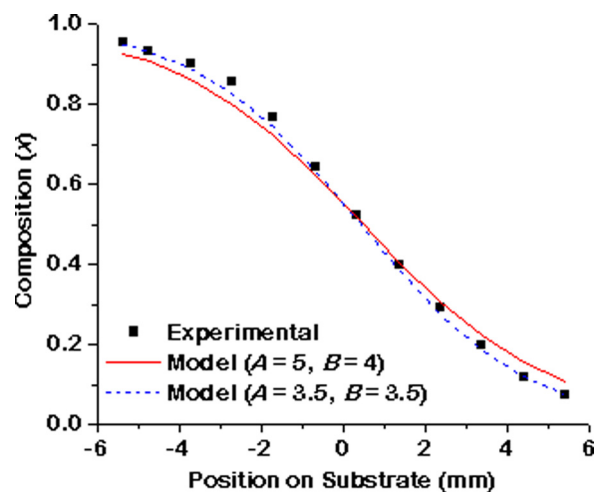


FIG. 11. (Color online) Composition profile for Cu in a 100 nm thick  $\text{Cu}_x\text{Pd}_{1-x}$  CSAF. Solid symbols represent the CSAF compositions at different points as measured from XPS experiments while the solid and the dotted lines represent the composition profiles estimated from the model for different positions of the source with respect to the substrate.  $A = 5$  mm and  $B = 4$  mm represent the nominal values of source-substrate position used during deposition.  $A = B = 3.5$  mm are the values obtained from the best fit of the deposition model to the data.

Figure 11 also illustrates the composition range accessed on this CSAF. The Cu mole fraction varies from  $x \sim 0.05$  to 0.95, meaning that this single CSAF contains all alloy compositions between  $\text{Cu}_{0.05}\text{Pd}_{0.95}$  and  $\text{Cu}_{0.95}\text{Pd}_{0.05}$ . In other words, the molar ratio of the components in the film varies by a factor of  $\sim 400$  across the CSAF. The spread of composition can be increased beyond  $\sim 0.05$  to 0.95 simply by choosing a slightly larger diameter substrate. The wide composition range is a result of our choice of line source operating temperatures that deliver similar Cu and Pd deposition rates. By changing the source temperatures, i.e., by changing relative deposit rates, we can choose to deposition CSAFs that span different regions of  $\text{Cu}_x\text{Pd}_{1-x}$  composition space.

Given the capacity of four line sources in the offset filament CSAF deposition source, it is possible to use this tool for preparation of ternary or quaternary CSAFs. Figure 12 illustrates the composition spread of a  $\text{Cu}_x\text{Au}_y\text{Pd}_{1-x-y}$  ternary CSAF. These concentration maps were obtained from a  $13 \times 13$  array of spatially resolved ( $200 \mu\text{m}$ ) XPS spectra obtained using a ThermoFisher ThetaProbe<sup>TM</sup>. The notation used to describe this ternary is  $\text{Cu}_{\min}^{\max}\text{Au}_{\min}^{\max}\text{Pd}_{\min}^{\max} = \text{Cu}_{2.7}^{79}\text{Au}_{9.1}^{59}\text{Pd}_{9.3}^{82}$  where *min* and *max* are the minimum and maximum concentrations each of the three components. The maximum concentrations of Cu, Au and Pd are in the lower right corner, top edge and lower left corner, respectively. In this case, the deposition rate of Au was lower than those of Cu and Pd resulting in a maximum Au concentration of 55% along the top edge of the CSAF. The

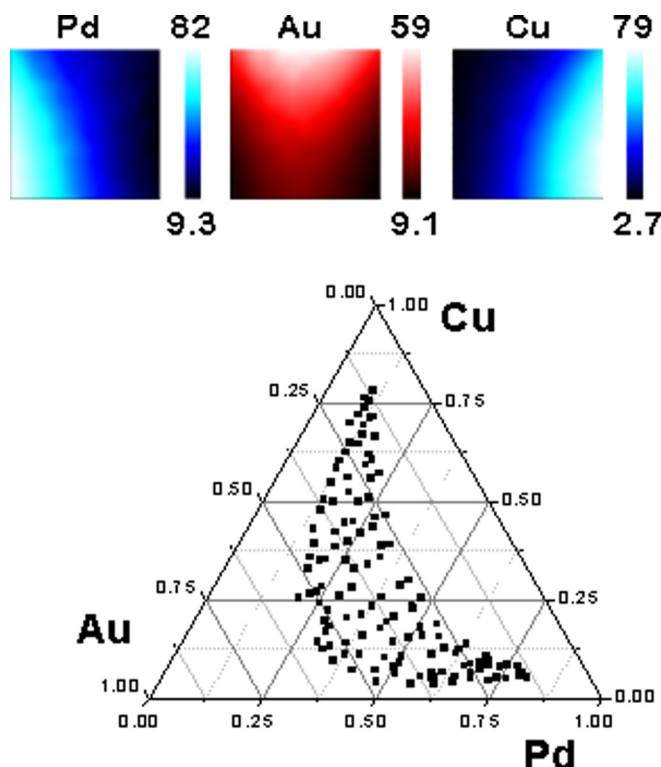


FIG. 12. (Color online) XPS maps of the concentrations of Cu, Au and Pd across a  $\text{Cu}_x\text{Au}_y\text{Pd}_{1-x-y}$  ternary CSAF. The minimum and maximum values of the compositions are given by  $\text{Cu}_{\min}^{\max}\text{Au}_{\min}^{\max}\text{Pd}_{\min}^{\max} = \text{Cu}_{2.7}^{79}\text{Au}_{9.1}^{59}\text{Pd}_{9.3}^{82}$ . The range of compositions as determined using XPS is shown in the ternary composition diagram.

spread of compositions on the  $\text{Cu}_x\text{Au}_y\text{Pd}_{1-x-y}$  CSAF is illustrated by the data points on the ternary composition diagram in Fig. 12.

### C. Assessment of the merits and limitations of the offset filament CSAF deposition tool

The offset filament deposition tool described in this work has a number of advantages over the methods illustrated in Fig. 2 for use in depositing CSAFs on small ( $\sim 1$  cm dia.) substrates. The lack of moving parts simplifies operation over the sliding contact mask [Fig. 2(a)] and allows deposition of multiple components simultaneously. The fact that the sources are lines allows them to be positioned very close to the edge of the substrate without the need for a shadow mask [Fig. 2(b)] to create the flux gradient across the substrate. This results in a very compact geometry; the entire source size is  $\sim 4 \times 4 \times 2 \text{ cm}^3$  mounted at the end of a water cooling tube that passes through a 2.75" conflate flange. Furthermore, the line sources eliminate the need for precise alignment of three separate objects: source, shadow and substrate. Conceptually, the line source deposition tool is similar to the method illustrated in Fig. 2(c). The fact that the sources are lines subtending very small angles in the direction along the substrate normal, allows them to be positioned close to the substrate while still giving a high flux gradient.

Needless to say there are limitations to the offset filament tool design. It is not appropriate for deposition of CSAFs across very large substrates. This is largely because the small volume of material in the line sources (a single straight 0.5 mm dia. wire) limits the total volume of material that can be deposited onto the substrate. It is also limited in the nature of the materials that can be deposited to form the components of the CSAF. The sources have been operated at temperatures as high as 1500 K for extended periods of time ( $> 10$  hs); however, the materials appropriate for deposition using these line sources must have vapor pressures high enough to yield useful fluxes at the center of the substrate ( $> 0.1$  nm/min) at temperatures below their melting points. Nonetheless, this includes quite a few elements among the alkali earths, first row transition metals, and noble metals.

### V. CONCLUSION

A simple, compact tool for deposition of CSAFs has been developed and demonstrated. Spatially resolved x ray photoemission was used to calibrate the deposition rates from Cu and Pd evaporative line sources. 100 nm  $\text{Cu}_x\text{Pd}_{1-x}$  CSAFs were prepared to demonstrate the performance of the deposition tool. Experimental measurements of compositions across the CSAF surface match those predicted by a simple model for the fluxes from the line sources to different locations on the substrate. Using deposition conditions that generate a  $\text{Cu}_{0.5}\text{Pd}_{0.5}$  alloy at the center of the substrate yields a binary CSAF that spans the composition range from  $\text{Cu}_{0.05}\text{Pd}_{0.95}$  to  $\text{Cu}_{0.95}\text{Pd}_{0.05}$ . CSAF libraries prepared using this deposition tool will enable rapid determination of composition-property relationships across continuous regions of alloy composition space.

## ACKNOWLEDGMENT

This technical effort was performed in support of the National Energy Technology Laboratory's ongoing research in Hydrogen Separation Membranes under the RES Grant No. DE-FE0004000.

- <sup>1</sup>I. Takeuchi, R. B. van Dover, and H. Koinuma, *MRS Bull.* **27**, 301 (2002).
- <sup>2</sup>S. I. Woo and S. H. Kim, *Top. Catal.* **53**, 1 (2010).
- <sup>3</sup>D. Priyadarshini, P. Kondratyuk, B. D. Morreale, A. J. Gellman, and J. B. Miller, *J. Phys. Chem. C* **115**, 10155 (2011).
- <sup>4</sup>J. C. Hogan, *Nat. Biotechnol.* **15**, 328 (1997).
- <sup>5</sup>J. P. Kennedy, L. Williams, T. M. Bridges, R. N. Daniels, D. Weaver, and C. W. Lindsley, *J. Comb. Chem.* **10**, 345 (2007).
- <sup>6</sup>J. Cui, Y. S. Chu, O. O. Famodu, Y. Faruya, J. Hatrick-Simpers, R. D. James, A. Ludwig, S. Thienhaus, M. Wuttig, Z. Zhang, and I. Takeuchi, *Nature Mat.* **5**, 286 (2006).
- <sup>7</sup>J. Wang and K. E. Gonsalves, *J. Comb. Chem.* **1**, 216 (1999).
- <sup>8</sup>J. N. Cawse, D. Olson, B. J. Chisholm, M. Brennan, T. Sun, W. Flanagan, J. Akhave, A. Mehrabi, and D. Saunders, *Prog. Org. Coat.* **47**, 128 (2003).
- <sup>9</sup>K. W. Kim, M. K. Jeon, K. S. Oh, T. S. Kim, Y. S. Kim, and S. I. Woo, *Proc. Natl. Acad. Sci. U.S.A.* **104**, 1134 (2007).
- <sup>10</sup>X. D. Xiang, X. Sun, G. Bricena, Y. Lou, K. A. Wang, H. Chang, W. G. Wallace-Freedman, S. W. Chen, and P. G. Schultz, *Science* **268**, 1738 (1995).
- <sup>11</sup>J. S. Cooper and P. J. McGinn, *Appl. Surf. Sci.* **254**, 662 (2007).
- <sup>12</sup>N. C. Woo, B. G. Ng, and R. B. V. Dover, *Rev. Sci. Instrum.* **78**, 072208 (2007).
- <sup>13</sup>O. L. Warren and T. J. Wyrobek, *Meas. Sci. Technol.* **16**, 100 (2005).
- <sup>14</sup>E. Danielson, J. H. Goldem, E. W. McFarland, C. M. Reaves, W. H. Weinberg, and X. D. Wu, *Nature Mat.* **389**, 944 (1997).
- <sup>15</sup>H. Koinuma and I. Takeuchi, *Nature Mat.* **3**, 429 (2004).
- <sup>16</sup>R. B. van Dover and L. F. Schneemeyer, *Macromol. Rapid Commun.* **25**, 150 (2004).
- <sup>17</sup>S. Guerin and B. E. Hayden, *J. Comb. Chem.* **8**, 66 (2006).
- <sup>18</sup>I. Ohkubo, H. M. Christen, P. Khalifah, S. Sathyamurthy, H. Y. Zhai, C. M. Rouleau, D. G. Mandrus, and D. H. Lowndes, *Appl. Surf. Sci.* **223**, 35 (2004).
- <sup>19</sup>Y. Yamada, T. Fukumura, M. Ikeda, M. Ohtani, H. Toyosaki, A. Ohtomo, F. Matsukura, H. Ohno, and M. Kawasaki, *J. Supercond.* **18**, 109 (2005).
- <sup>20</sup>M. Bate, C. Neuber, R. Giesa, and H.-W. Schmidt, *Macromol. Rapid Commun.* **25**, 371 (2004).
- <sup>21</sup>R. Dell'Anna, P. Lazzeri, R. Canteri, C. J. Long, L. Hatrick-Simpers, I. Takeuchi, and M. Anderle, *QSAR Comb. Sci.* **27**, 171 (2008).
- <sup>22</sup>C. Gao, B. Hu, I. Takeuchi, K. S. Chang, X. D. Xiang, and G. Wang, *Meas. Sci. Technol.* **16**, 248 (2005).
- <sup>23</sup>R. F. Egerton and J. C. Bennett, *J. Microsc.* **183**, 116 (1996).
- <sup>24</sup>K. Kennedy, T. Stefansky, G. Davy, V. F. Zacky, and E. R. Parker, *J. Appl. Phys.* **36**, 3808 (1965).
- <sup>25</sup>C. Park, E. Bauer, and H. Poppa, *Surf. Sci.* **154**, 371 (1985).
- <sup>26</sup>J. W. He, W. L. Shea, X. Xiang, and D. W. Goodman, *J. Vac. Sci. Technol. A* **8**, 2435 (1990).
- <sup>27</sup>J. B. Miller, C. Matranga, and A. J. Gellman, *Surf. Sci.* **602**, 375 (2008).
- <sup>28</sup>P. J. Cumpson and M. P. Seah, *Surf. Interface Anal.* **25**, 430 (1997).
- <sup>29</sup>H. Hertz, *Ann. Phys.* **17**, 177 (1882).
- <sup>30</sup>M. Knudsen, *Ann. Phys.* **47**, 697 (1915).
- <sup>31</sup>P. Rahimi and C. A. Ward, *Int. J. Thermodyn.* **8**, 1 (2005).